nature nanotechnology

LETTERS

PUBLISHED ONLINE: 23 MARCH 2015 | DOI: 10.1038/NNANO.2015.36

Graphene-templated directional growth of an inorganic nanowire

Won Chul Lee[1,2†], Kwanpyo Kim[3,4†], Jungwon Park[5,6†], Jahyun Koo[7], Hu Young Jeong[8], Hoonkyung Lee[7], David A. Weitz[5,6], Alex Zettl[3,9*] and Shoji Takeuchi[1,2*]

Assembling inorganic nanomaterials on graphene[1–3] is of interest in the development of nanodevices and nanocomposite materials, and the ability to align such inorganic nanomaterials on the graphene surface is expected to lead to improved functionalities[4], as has previously been demonstrated with organic nanomaterials epitaxially aligned on graphitic surfaces[5–10]. However, because graphene is chemically inert, it is difficult to precisely assemble inorganic nanomaterials on pristine graphene[2,11–16]. Previous techniques[2,3] based on dangling bonds of damaged graphene[11,17–20], intermediate seed materials[11,15,16,21,22] and vapour-phase deposition at high temperature[12–14,23–25] have only formed randomly oriented or poorly aligned inorganic nanostructures. Here, we show that inorganic nanowires of gold(I) cyanide can grow directly on pristine graphene, aligning themselves with the zigzag lattice directions of the graphene. The nanowires are synthesized through a self-organized growth process in aqueous solution at room temperature, which indicates that the inorganic material spontaneously binds to the pristine graphene surface. First-principles calculations suggest that this assembly originates from lattice matching and π interaction to gold atoms. Using the synthesized nanowires as templates, we also fabricate nanostructures with controlled crystal orientations such as graphene nanoribbons with zigzag-edged directions.

The nanowires were synthesized by incubating single-layered graphene and solid gold simultaneously in an aqueous solution of 250 mM ammonium persulphate, $(NH_4)_2S_2O_8$, at room temperature for 17 h (Fig. 1a). Various types of gold precursor, such as gold nanoparticles or gold microstructures, can be used in this reaction depending on the experimental goal. The acidic solution of ammonium persulphate oxidizes gold precursors to form nanowires. Graphene, as both a substrate and template for nanowire growth, is floated on the reaction solution, thus providing a surface on which the nucleation and growth of nanowires can occur (Supplementary Methods and Supplementary Fig. 1).

During this incubation, the nanowires grow on the graphene surfaces along the specific lattice directions of the graphene. Typical transmission electron microscopy (TEM) images of the graphene/nanowire samples (Fig. 1b and Supplementary Fig. 2a,b) show horizontally grown nanowires on the surfaces. Measurements obtained using TEM and atomic force microscopy (AFM) indicate that the nanowires are in the form of nanoribbons lying on the graphene surfaces, with length, width and thickness of 94.7 ± 42.2 nm, 10.1 ± 5.0 nm and 3.29 ± 0.47 nm, respectively (Supplementary Fig. 3). Interestingly, the synthesized nanowires are preferentially oriented along three directions with rotations of 120° relative to one another (Fig. 1b and Supplementary Fig. 2a–d). From the observed symmetry of the nanowire axis directions, we expected the nanowires to have preferential growth directions that are related to the underlying graphene lattice structures. Indeed, a selected area electron diffraction (SAED) pattern (inset in Fig. 1b) of the samples clearly shows this epitaxial relationship between the nanowires and graphene. The nanowire axis directions in Fig. 1b show good orientational alignment to the second-order diffraction peaks—(1–210) peaks—of graphene (circled in red). This alignment, which is also confirmed statistically (Fig. 1d), indicates that the nanowire directions coincide with the zigzag lattice directions of the underlying graphene in real lattice space. In addition, the diffraction peaks from the nanowires (circled in yellow) are aligned to graphene's (1–210) peaks in the SAED pattern. Together with high-resolution TEM images and their Fourier transforms (Fig. 1c and Supplementary Fig. 2e,f), the SAED pattern shows that each nanowire is single crystalline and that the crystal lattices of the nanowires and graphene are rotationally aligned. An atomic-resolution TEM image (Fig. 1e,f) also directly confirms the nanowire alignment on the graphene, with the nanowire axis aligned along the zigzag lattice direction of the graphene lattice.

This nanowire alignment enables us to easily visualize the crystal directions and grain boundaries in polycrystalline graphene using TEM or even scanning electron microscopy (SEM), as shown in Fig. 1g,h. Because the nanowire axes directly represent the crystal directions of the underlying graphene, tilt grain boundaries in the graphene can be identified by changes in the nanowire axis directions (Fig. 1i). Previously, atomic-resolution imaging tools such as TEM and scanning tunnelling microscopy (STM) have been used to directly image the crystal directions and grain boundaries of graphene[26]. However, these imaging processes often involve special sample preparation or substrate requirements and can be time-consuming. The present SEM-based imaging provides a facile tool to monitor crystal directions and graphene grain boundaries (with a spatial resolution of ~100 nm in Supplementary Fig. 4), which is essential for studying the polycrystallinity of graphene and its implications for various properties.

We identified the nanowire material as gold(I) cyanide[27] (AuCN) based on our elemental analysis and atomic structure characterizations. Elemental analyses including energy-dispersive X-ray spectroscopy (EDX) and electron energy loss spectroscopy (EELS) (Supplementary Figs 5 and 6) confirm the presence of Au and N,

[1]Institute of Industrial Science, The University of Tokyo, Tokyo 153-8505, Japan. [2]ERATO Takeuchi Biohybrid Innovation Project, Japan Science and Technology Agency, Tokyo 153-8904, Japan. [3]Department of Physics, University of California at Berkeley, Berkeley, California 94720, USA. [4]Department of Physics, Ulsan National Institute of Science and Technology (UNIST), Ulsan 689-798, South Korea. [5]School of Engineering and Applied Sciences, Harvard University, Cambridge, Massachusetts 02138, USA. [6]Department of Physics, Harvard University, Cambridge, Massachusetts 02138, USA. [7]Department of Physics, Konkuk University, Seoul 143-701, South Korea. [8]UNIST Central Research Facilities (UCRF), Ulsan National Institute of Science and Technology (UNIST), Ulsan 689-798, South Korea. [9]Materials Sciences Division, Lawrence Berkeley National Laboratory, Berkeley, California 94720, USA. †These authors contributed equally to this work. *e-mail: takeuchi@iis.u-tokyo.ac.jp; azettl@berkeley.edu

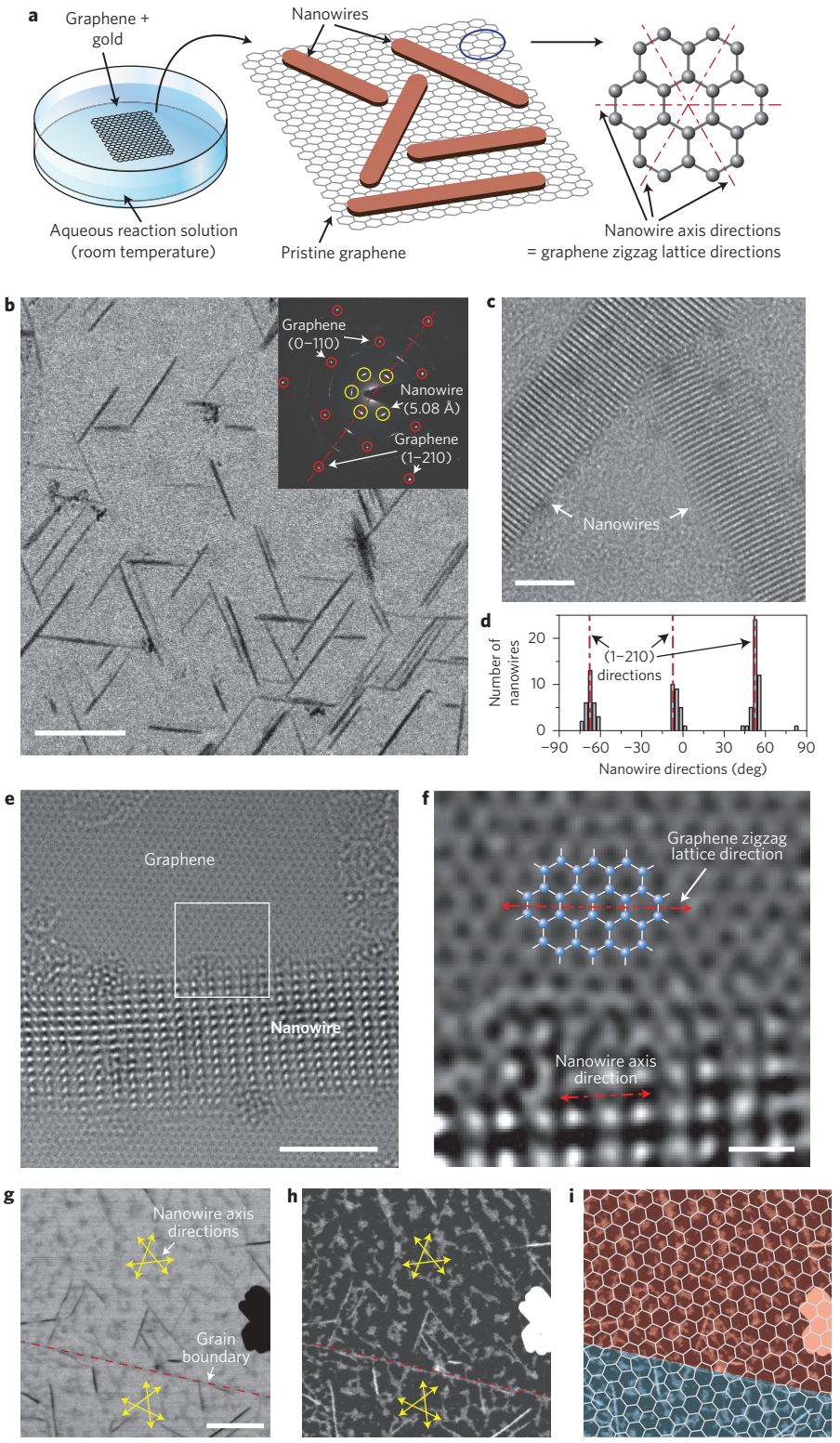

Figure 1 | Directional growth of inorganic nanowires on graphene. a, Schematic of the process. An aqueous-phase reaction at room temperature results in nanowires whose axes are parallel to the zigzag lattice directions of pristine graphene. **b**, TEM image of the synthesized nanowires on graphene. Scale bar, 100 nm. Inset: SAED pattern of the nanowire–graphene sample. The nanowire axes are aligned to the zigzag lattice directions (the (1–210) directions) of graphene. **c**, High-resolution TEM image of the nanowires. Scale bar, 5 nm. **d**, Histogram of the angular distributions of the nanowire axes in **b**. **e**, Atomic-resolution TEM image of a nanowire on graphene. Scale bar, 3 nm. **f**, Enlarged view of box in **e**. Low-pass filtering (cutoff: four pixels) is applied to remove high-frequency noise. The directional alignment of the nanowire axis with the graphene zigzag lattice direction is clearly observed. Scale bar, 0.5 nm. **g–i**, Using the nanowires to image the crystal directions and domain boundaries of polycrystalline graphene. The same specimen area is imaged with TEM (**g**) and SEM (**h**). The graphene lattice directions can be identified using the nanowire axis directions. Scale bar, 100 nm. In **i**, the SEM image (**h**) is shown with an overlay of the pseudo-lattice structures of graphene. The red and blue colour maps represent different domains with relatively tilted lattice directions.

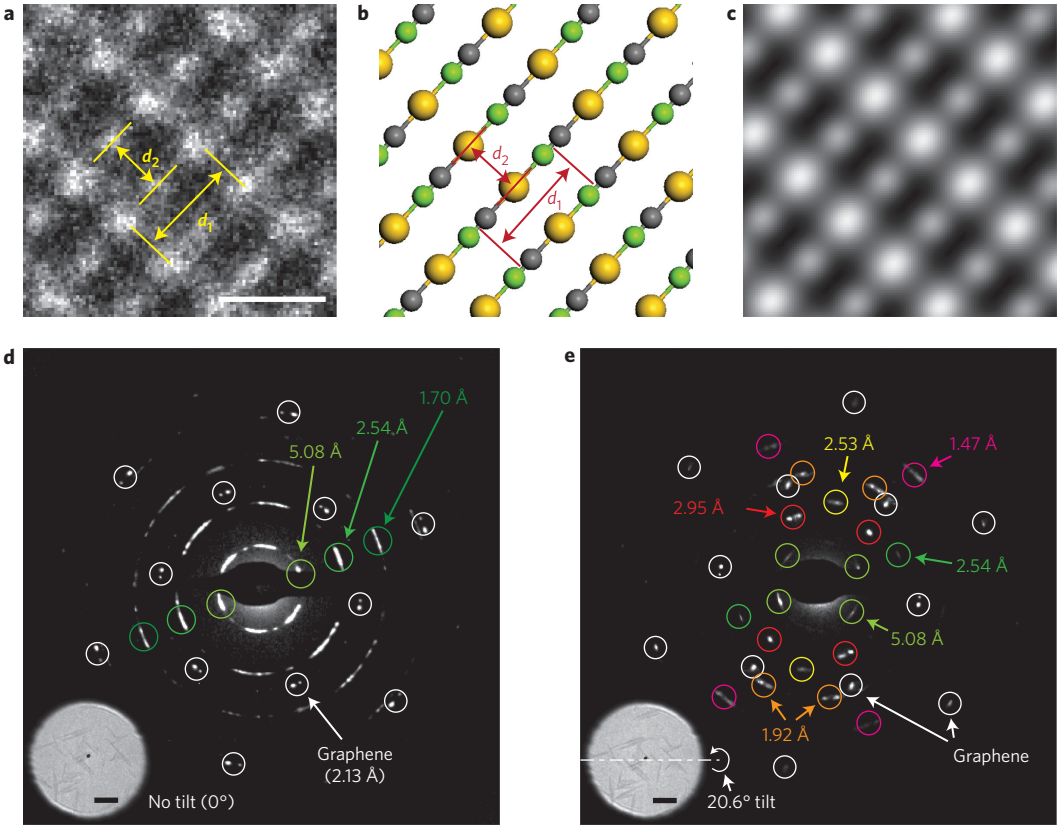

Figure 2 | Atomic-resolution TEM imaging and SAED of the nanowires. a, Atomic-resolution TEM image of the nanowire. The two lattice spacings along (d_1) and perpendicular (d_2) to the nanowire axis direction are measured as 5.08 ± 0.01 Å and 3.00 ± 0.12 Å, respectively. A TEM image of a larger area is provided in Supplementary Fig. 7. Scale bar, 0.5 nm. **b**, Crystal structure of AuCN. The yellow, green and grey spheres represent Au, N and C atoms, respectively. Lattice spacings d_1 and d_2 obtained from the crystal structure are 5.091 Å and 2.937 Å, respectively. **c**, Simulated TEM image from the crystal structure in **b**. The captured TEM image (**a**), crystal structure (**b**) and simulated TEM image (**c**) show good agreement. **d**,**e**, SAED patterns of a nanowire–graphene sample under no tilt (**d**) and 20.6° tilt (**e**). Insets: Sample areas where the SAED patterns are measured. Scale bars (**d**,**e**), 100 nm.

as well as non-graphene C (and a trace amount of H) between all potential constituent elements from the precursor solution (Supplementary Section 'Elemental analysis'). Atomic-resolution TEM imaging (Fig. 2a and Supplementary Fig. 7) and SAED from multiple imaging axes (Fig. 2d,e and Supplementary Fig. 8) allow us to precisely determine the crystal structure. The atomic-resolution TEM images including Fig. 2a directly show unique atomic structures with two orthogonal lattice spacings of 5.08 ± 0.01 Å (d_1) and 3.00 ± 0.12 Å (d_2), which correspond to AuCN's hexagonal crystal[27] (5.091 Å and 2.937 Å). Indeed, AuCN is the sole material candidate that satisfies the observed crystal symmetry and lattice spacings of all the reported inorganic compounds composed of the possible constituent elements (Au, N, C and/or H) classified from the spectroscopic elemental analysis. We further confirmed that the post-simulated TEM image (Fig. 2c) of an AuCN crystal (Fig. 2b) reproduces the unique crystal patterns observed in the experimental TEM images. Most importantly, SAED with multiple imaging axes confirms that the nanowire crystal is AuCN. Owing to the nature of the alignment between the nanowires and graphene, SAED patterns from nanowires with no specimen tilting only display the specific *d*-spacing (5.08 Å) and its high-order peaks from a [100] zone axis (Fig. 2d and Supplementary Fig. 8a). Tilting multiple nanowires within the field of view allows us to investigate a set of SAED peaks from various zone axes and to precisely obtain three-dimensional structural information (Fig. 2e and Supplementary Fig. 8b). All the *d*-spacings measured from the SAED patterns of the nanowires coincide well with those of AuCN (Supplementary Fig. 8c).

The crystal structure also reveals the alignment mechanism between the nanowires and graphene. Because it is well known that lattice matching between two materials causes heteroepitaxial alignment[13,14,24], we compared the in-plane atomic configurations of the nanowires and graphene (Fig. 3a). Along the nanowire axis directions, the unit cell size (d_1) of AuCN (5.08 ± 0.01 Å) coincides well with the length of two carbon hexagons (4.92 Å) along the graphene zigzag directions (lattice mismatch = 3.3 ± 0.2%). In the nanowire width directions, the unit cell sizes ($6d_2$) of AuCN (18.00 ± 0.72 Å) and graphene (19.17 Å) are also matched (lattice mismatch = 6.1 ± 3.8%). Note that the epitaxial alignment of inorganic materials on graphene is successful with a lattice mismatch of ~2.9% (Bi_2Se_3 on graphene[13]), and is possible even with a lattice mismatch of ~28% (MoS_2 on graphene[24]). Thus, in-plane lattice matching is mainly responsible for the epitaxial alignment between the AuCN nanowires and graphene.

We also confirmed that the AuCN nanowires are likely to form directly on pristine surfaces of graphene, although other inorganic materials preferentially attach to dangling bonds such as graphene edges and defects[2,11,13–17]. First, the Raman spectra of graphene before and after nanowire synthesis (Supplementary Fig. 9a,b) maintain very low D peaks, indicating that the graphene is of high quality and measurable defects are not introduced during the nanowire synthesis process. Second, atomic-resolution TEM imaging directly shows the pristine state of the graphene underneath the nanowires. We stripped a nanowire off (Supplementary Fig. 9c,d) and observed a clean graphene lattice without any visible defects (Supplementary Fig. 9e). Third, we synthesized nanowires on

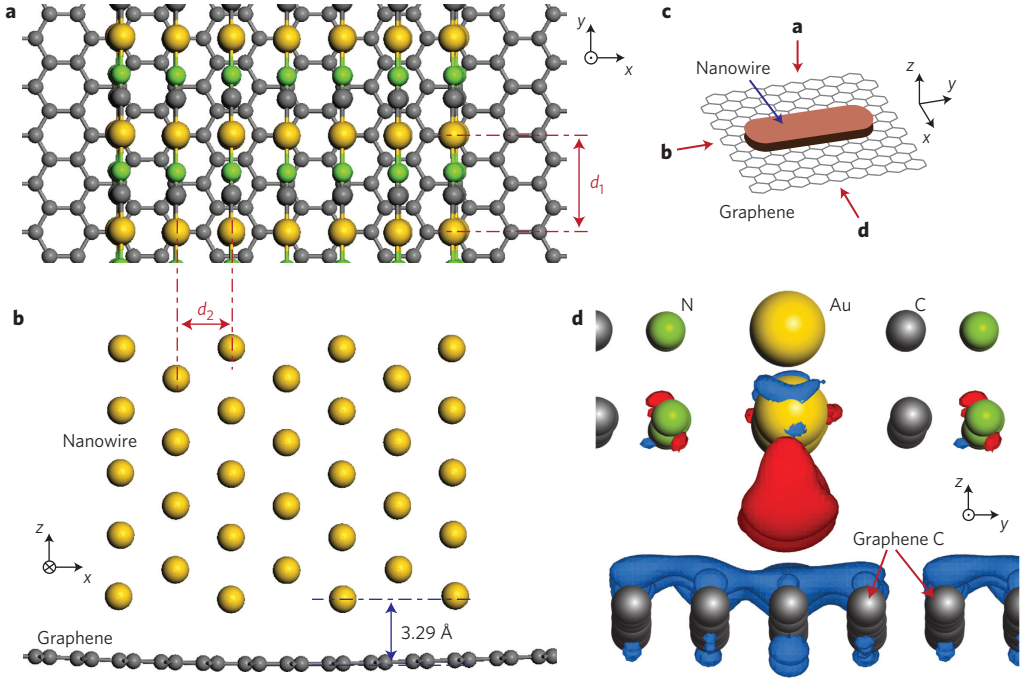

Figure 3 | Interaction between the nanowire and graphene estimated by first-principles calculations. a,**b**, Optimized atomic configuration of the nanowire and graphene estimated by first-principles calculations: plan view from the top (**a**) and side view from the nanowire-axis direction (**b**). **c**, Schematic view of the nanowire and graphene. Red arrows represent the viewing orientations of the panels. **d**, Molecular structures with an overlay of charge density difference isosurfaces at the nanowire–graphene interface. The red and blue charge density difference isosurfaces are contoured at the level of ±0.0004 e Å^{-3}, indicating electron accumulation and depletion, respectively.

sub-monolayer graphene samples consisting of domains that were disconnected from each other. The sub-monolayer graphene, when transferred onto amorphous carbon films of TEM grids, provides three different types of carbon surface for nanowire growth: pristine graphene in the middle of the domains, graphene defects at the edge of the domains, and amorphous carbon (from TEM grids) outside the domains. During synthesis, no nanowire is formed on amorphous carbon surfaces and the nanowire density is uniform throughout the graphene domains and edges (Supplementary Fig. 9f–h). These results imply that the nanowires grow preferentially on pristine graphene surfaces (not on graphene defects) and do not perturb the crystal structure of the graphene. Moreover, the third experiment (Supplementary Fig. 9f–h) indicates that graphene is a unique substrate promoting the formation of uncommon inorganic crystals. As also shown by the synthesis of new organic crystals on graphene[5,7,8], this result suggests the possibility of using graphene as a template for advanced nanostructuring of inorganic materials.

The nanowire growth on pristine graphene suggests that the interaction between the two materials is unusual for inorganic materials. Owing to the chemical inertness of graphene, the only way previously shown to synthesize inorganic structures directly on pristine graphene has been vapour-phase deposition[12–14,23–25], which is mainly performed at high temperatures (400–900 °C). However, the reaction in this study occurs in the aqueous phase at room temperature, which suggests that the interaction between the nanowires and pristine graphene provides a sufficient driving force for assembly without high energy. Thus, we investigated the interaction between the nanowires and graphene using first-principles calculations (Supplementary Methods). In the optimized atomic configuration (Fig. 3a,b), both AuCN's hexagonal crystal and graphene's sp^2 carbon structures remain intact, and their interlayer distance (3.29 Å) is almost the same as the interlayer distance (3.31 Å) between Au(111) and graphene[28]. The parallel atomic structure at the interface (Fig. 3b,d) suggests that Au atoms, whose covalent radius (1.3 Å) is significantly larger than those of C and N (0.7 Å), contribute predominantly to the interaction between the nanowire and graphene. The major binding contribution of Au atoms is also confirmed in the charge density difference (Fig. 3d), where transferred electrons are localized only near Au atoms. However, the interaction between graphene and Au atoms in AuCN has unique characteristics that differ from the common physical interaction between graphene and Au(111). The calculated binding energy of AuCN on graphene is 181 meV/Au, significantly greater than the 80 meV/Au for the binding energy between Au (111) and graphene via electrostatic interaction[28]. The charge density difference (Fig. 3d) shows that the π orbitals of graphene donate electrons to Au atoms in AuCN. These characteristics support the notion that the nanowire– graphene interaction is mainly attributed to electron transfer between a transition metal (Au) and cyclic π systems. This type of interaction, previously studied in organometallic chemistry, differs from the relatively weak physisorption[2,14,28] (either electrostatic or van der Waals interaction) that is commonly observed at interfaces between inorganic crystals and graphene. We note that the organometallic π interaction with graphene has been found with only a few inorganic materials[29], which are not even crystals but molecules. The unique π interaction is presumably responsible for the spontaneous binding between the nanowires and graphene, and it also offers the possibility of synthesizing various inorganic materials on pristine graphene without disturbing sp^2 carbon networks[2,29].

The as-prepared nanowires allowed us to fabricate nanostructures with controlled crystallographic orientations (Fig. 4a). First, graphene nanoribbons with zigzag-edged directions (which can be important components in spintronic devices[30]) were fabricated using the synthesized nanowires as an etching mask. The nanowire-covered graphene was selectively protected from O_2 plasma etching (Fig. 4b), and the nanowires were then removed with a

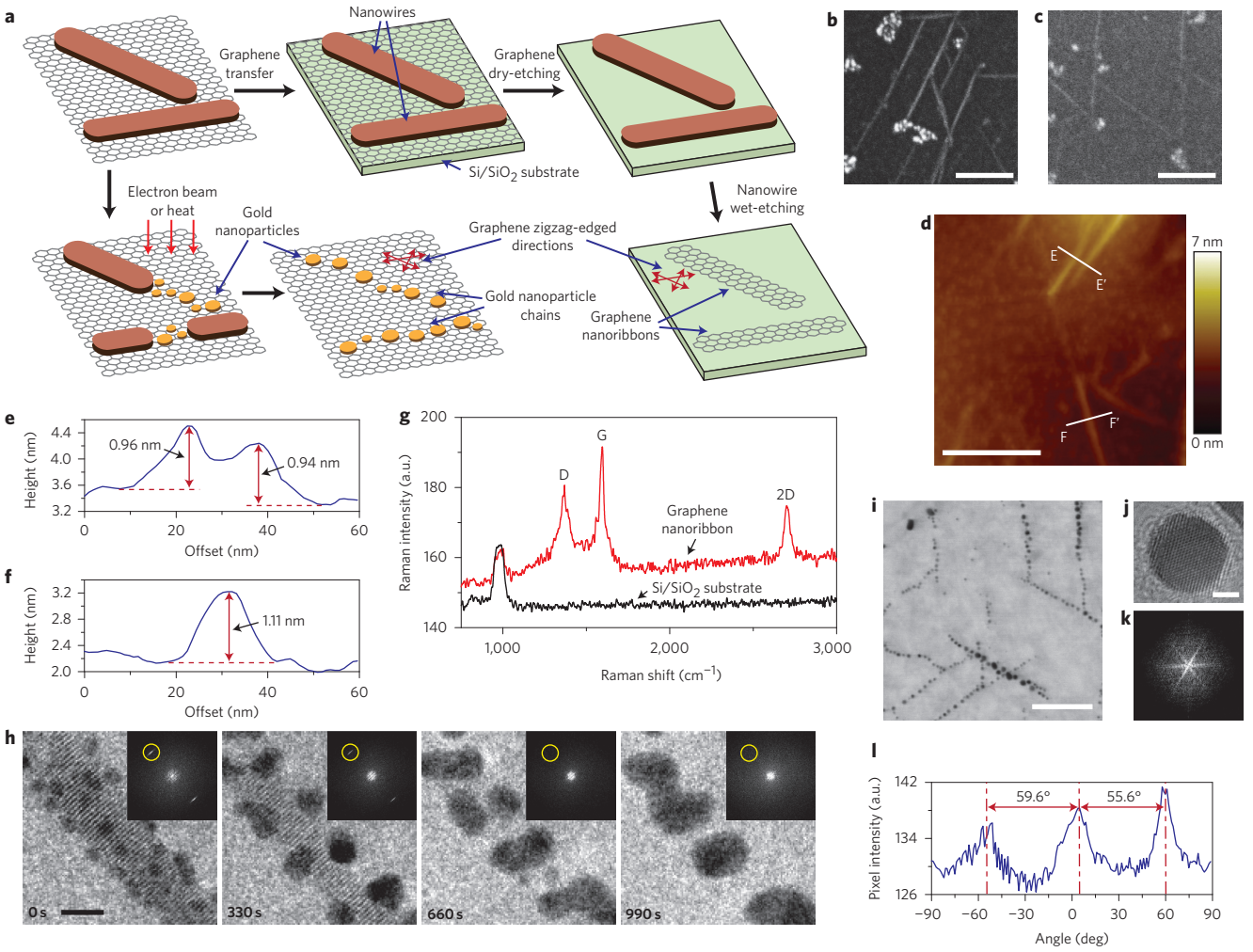

Figure 4 | Fabrication of crystallographically aligned nanostructures. a, Fabrication process for the graphene nanoribbons and gold nanoparticle chains based on the nanowires aligned on graphene. **b**,**c**, SEM images of the nanowires after graphene dry-etching (**b**) and the fabricated graphene nanoribbons (**c**), which are aligned with the zigzag lattice directions. Scale bars, 100 nm. **d**, AFM image of the graphene nanoribbons. Scale bar, 100 nm. **e**,**f**, Height profiles of the sample along E–E′ (**e**) and F–F′ (**f**) in **d**. **g**, Raman spectrum of the fabricated graphene nanoribbons (red line). The negative control signal (black line) is measured from a position where the graphene is fully etched out in the same sample. **h**, A series of TEM images from Supplementary Movie 1 showing the nanowire decomposition process to gold nanoparticle chains under electron-beam irradiation. Insets: Fourier transforms of the TEM images. Scale bar, 5 nm. **i**, Gold nanoparticle chains formed by thermal decomposition of nanowires. Scale bar, 100 nm. **j**, High-resolution TEM image of a gold nanoparticle in the chain. Scale bar, 2 nm. **k**, Fourier transform of **i**. The directions of the bright lines are orthogonal to the axis directions of the gold nanoparticle chains. **l**, Radial pixel intensities of **k**, averaged along a line from the centre at different angles. The directional alignment of the gold nanoparticle chains is shown with inter-peak angles of ~60°.

NaOH solution without damaging the graphene (Fig. 4c and Supplementary Fig. 10). Because the nanowires are conformally attached on the graphene and their widths can be controlled to within less than 10 nm, the present method readily enables us to fabricate graphene nanoribbons with sub-10 nm widths. The AFM image in Fig. 4d and its height profiles (Fig. 4e,f) indicate that the widths of the fabricated graphene nanoribbons are near 10 nm, with the tip-size effect taken into account. In addition, the thickness of the fabricated graphene nanoribbon is ~1 nm, which is consistent with the reported thickness[31] of single-layered graphene on SiO_2. The Raman spectrum (Fig. 4g) also indicates that the graphene nanoribbons are fabricated successfully. The intensity ratio of the D and G bands (I_D/I_G), a common measure to evaluate the quality of carbon materials, is ~0.67, which is advanced for graphene nanoribbons produced by top-down fabrication. Overall, the AFM and Raman data indicate that the fabricated graphene nanoribbons are of reasonable quality (in particular the edge smoothness) compared to previously available graphene nanoribbons[31]. The crucial point in this fabrication process is that the directional alignment of the nanowires allows us to selectively fabricate graphene nanoribbons in zigzag-edged directions. Note that it has been difficult to fabricate graphene nanoribbons with zigzag-edged directions and only a few previous studies[32] have achieved it so far.

As the second example of crystallographically aligned nanostructures we fabricated gold nanoparticle chains aligned to the crystal directions of graphene substrates by decomposing the nanowires to gold nanoparticles (Fig. 4a). The electron beam in TEM was used to decompose the synthesized nanowires on graphene (Supplementary Movie 1 and Fig. 4h). Gold nanoparticles (dark dots) grow near the nanowire and finally replace the entire nanowire (Supplementary Fig. 11). The application of heat (200 °C, 30 min) can also decompose the nanowires to gold nanoparticles (Fig. 4i,j). Because the nanowire arrangement determines the position of the gold nanoparticle, the gold nanoparticle chains are naturally aligned along the zigzag lattice directions of the graphene substrate (Fig. 4k,l). These gold nanoparticle chains are in the

optimal dimension for near-field plasmon coupling[33], which can propagate and/or enhance the electromagnetic waves of applied light along the chain axes. Thus, light with a particular wavelength and polarization will interact strongly along specific crystal directions of the graphene. This phenomenon suggests potential applications in optical measurements of graphene crystal directions and plasmonic sensing platforms.

In summary, we have presented the self-organized growth of inorganic AuCN nanowires that are readily aligned to the zigzag lattice directions of single-layered pristine graphene. This direct alignment can be utilized to extract and control crystallographic information about nanostructures, thus enabling us to fabricate graphene nanoribbons with zigzag-edged directions. The synthetic method we have introduced demonstrates the possibility of using graphene as a template for advanced classes of inorganic nanomaterials, even with wet chemistry. Furthermore, the unique interaction found in this study may provide a new direction for the fabrication of graphene–inorganic heterostructures with intrinsic interface properties.

Received 14 May 2014; accepted 9 February 2015;
published online 23 March 2015

References

1. Geim, A. K. & Grigorieva, I. V. Van der Waals heterostructures. *Nature* **499,** 419–425 (2013).
2. Georgakilas, V. *et al.* Functionalization of graphene: covalent and non-covalent approaches, derivatives and applications. *Chem. Rev.* **112,** 6156–6214 (2012).
3. Huang, X., Qi, X., Boey, F. & Zhang, H. Graphene-based composites. *Chem. Soc. Rev.* **41,** 666–686 (2012).
4. Barth, J. V., Costantini, G. & Kern, K. Engineering atomic and molecular nanostructures at surfaces. *Nature* **437,** 671–679 (2005).
5. Hong, G. *et al.* Recent progress in organic molecule/graphene interfaces. *Nano Today* **8,** 388–402 (2013).
6. Kim, D. W., Kim, Y. H., Jeong, H. S. & Jung, H-T. Direct visualization of large-area graphene domains and boundaries by optical birefringency. *Nature Nanotech.* **7,** 29–34 (2012).
7. Garnica, M. *et al.* Long-range magnetic order in a purely organic 2D layer adsorbed on epitaxial graphene. *Nature Phys.* **9,** 368–374 (2013).
8. Colson, J. W. *et al.* Oriented 2D covalent organic framework thin films on single-layer graphene. *Science* **332,** 228–231 (2011).
9. Zhang, F. *et al.* Epitaxial growth of peptide nanofilaments on inorganic surfaces: effects of interfacial hydrophobicity/hydrophilicity. *Angew. Chem. Int. Ed.* **45,** 3611–3613 (2006).
10. Fukushima, T. *et al.* Molecular ordering of organic molten salts triggered by single-walled carbon nanotubes. *Science* **300,** 2072–2074 (2003).
11. Chung, K., Lee, C-H. & Yi, G-C. Transferable GaN layers grown on ZnO-coated graphene layers for optoelectronic devices. *Science* **330,** 655–657 (2010).
12. Addou, R., Dahal, A. & Batzill, M. Growth of a two-dimensional dielectric monolayer on quasi-freestanding graphene. *Nature Nanotech.* **8,** 41–45 (2013).
13. Dang, W., Peng, H., Li, H., Wang, P. & Liu, Z. Epitaxial heterostructures of ultrathin topological insulator nanoplate and graphene. *Nano Lett* **10,** 2870–2876 (2010).
14. Hong, Y. J. *et al.* Van der Waals epitaxial double heterostructure: InAs/single-layer graphene/InAs. *Adv. Mater.* **25,** 6847–6853 (2013).
15. Wang, X., Tabakman, S. M. & Dai, H. Atomic layer deposition of metal oxides on pristine and functionalized graphene. *J. Am. Chem. Soc.* **130,** 8152–8153 (2008).
16. Alaboson, J. M. P. *et al.* Templating sub-10 nm atomic layer deposited oxide nanostructures on graphene via one-dimensional organic self-assembled monolayers. *Nano Lett.* **13,** 5763–5770 (2013).
17. Kim, K. *et al.* Selective metal deposition at graphene line defects by atomic layer deposition. *Nature Commun.* **5,** 4781 (2014).
18. Liang, Y. *et al.* Co_3O_4 nanocrystals on graphene as a synergistic catalyst for oxygen reduction reaction. *Nature Mater.* **10,** 780–786 (2011).
19. Si, Y. & Samulski, E. T. Exfoliated graphene separated by platinum nanoparticles. *Chem. Mater.* **20,** 6792–6797 (2008).
20. Lightcap, I. V., Kosel, T. H. & Kamat, P. V. Anchoring semiconductor and metal nanoparticles on a two-dimensional catalyst mat. Storing and shuttling electrons with reduced graphene oxide. *Nano Lett.* **10,** 577–583 (2010).
21. Choi, D. *et al.* Fully rollable transparent nanogenerators based on graphene electrodes. *Adv. Mater.* **22,** 2187–2192 (2010).
22. Huang, X. *et al.* Reduced graphene oxide-templated photochemical synthesis and *in situ* assembly of Au nanodots to orderly patterned Au nanodot chains. *Small* **6,** 513–516 (2010).
23. Kumar, B. *et al.* Controlled growth of semiconducting nanowire, nanowall, and hybrid nanostructures on graphene for piezoelectric nanogenerators. *ACS Nano* **5,** 4197–4204 (2011).
24. Shi, Y. *et al.* Van der Waals epitaxy of MoS_2 layers using graphene as growth templates. *Nano Lett.* **12,** 2784–2791 (2012).
25. Zhou, H. *et al.* The transformation of a gold film on few-layer graphene to produce either hexagonal or triangular nanoparticles during annealing. *Carbon* **52,** 379–387 (2013).
26. Kim, K. *et al.* Grain boundary mapping in polycrystalline graphene. *ACS Nano* **5,** 2142–2146 (2011).
27. Hibble, S. J., Hannon, A. C. & Cheyne, S. M. Structure of AuCN determined from total neutron diffraction. *Inorg. Chem.* **42,** 4724–4730 (2003).
28. Giovannetti, G. *et al.* Doping graphene with metal contacts. *Phys. Rev. Lett.* **101,** 026803 (2008).
29. Sarkar, S. *et al.* Organometallic hexahapto functionalization of single layer graphene as a route to high mobility graphene devices. *Adv. Mater.* **25,** 1131–1136 (2013).
30. Son, Y-W., Cohen, M. L. & Louie, S. G. Half-metallic graphene nanoribbons. *Nature* **444,** 347–349 (2006).
31. Jiao, L., Zhang, L., Wang, X., Diankov, G. & Dai, H. Narrow graphene nanoribbons from carbon nanotubes. *Nature* **458,** 877–880 (2009).
32. Shi, Z. *et al.* Patterning graphene with zigzag edges by self-aligned anisotropic etching. *Adv. Mater.* **23,** 3061–3065 (2011).
33. Halas, N. J., Lal, S., Chang, W. S., Link, S. & Nordlander, P. Plasmons in strongly coupled metallic nanostructures. *Chem. Rev.* **111,** 3913–3961 (2011).

Acknowledgements

The authors thank A.P. Alivisatos, H. Fujita, Y. Arakawa, B.J. Kim, L. Yang, J. Moon, Y. Ota, H. Suh, J. Kwon and J. Min for helpful discussions. The authors also thank J. Kim and Y. Mizutani for the AFM analysis, S. Mori and M. Onuki for technical support and A. Sato for help with graphic illustrations. This work was mainly supported by the Takeuchi Biohybrid Innovation Project, Exploratory Research for Advanced Technology (ERATO), Japan Science and Technology (JST). A.Z. and K.K. acknowledge support from the Director, Office of Energy Research, Materials Sciences and Engineering Division, of the US Department of Energy (DE-AC02-05CH11231) and from the Office of Naval Research (MURI grant N00014-09-1066). K.K. also acknowledges support from the Basic Science Research Program through the National Research Foundation of Korea (NRF) funded by the Ministry of Education (NRF-2014R1A1A2058178). D.A.W. and J.P. acknowledge support from the Harvard MRSEC (DMR-0820484) and Amore-Pacific. H.L. and J.K. acknowledge support from the Basic Science Research Program through the National Research Foundation of Korea, funded by the Ministry of Science, ICT & Future Planning (NRF-2015R1A1A1001583) and also acknowledge support from KISTI under the Supercomputing Applications Support Program (KSC-2013-C3-034). H.Y.J. acknowledges support from the 2012 Research Fund (1.120032.01) of UNIST.

Author contributions

W.C.L., K.K. and J.P. conceived the design of the study. S.T., A.Z. and D.A.W. supervised the project. K.K. and J.P. initially discovered the nanowire synthesis phenomenon. W.C.L., K.K., J.P. and H.Y.J. performed all experiments. J.K. and H.L. performed first-principles calculations. W.C.L., K.K., J.P., H.L., D.A.W., A.Z. and S.T. wrote the manuscript. All authors discussed the results and commented on the manuscript.

Additional information

Supplementary information is available in the online version of the paper. Reprints and permissions information is available online at www.nature.com/reprints. Correspondence and requests for materials should be addressed to A.Z. and S.T.

Competing financial interests

The authors declare no competing financial interests.